ISSN 1990-7478, Biochemistry (Moscow), Supplement Series A: Membrane and Cell Biology, 2017, Vol. 11, No. 2, pp. 151–167. © Pleiades Publishing, Ltd., 2017.
Original Russian Text © E.M. Novikova, V.A. Vodeneev, V.S. Sukhov, 2017, published in Biologicheskie Membrany, 2017, Vol. 34, No. 2, pp. 109–125.

ARTICLES

Mathematical Model of Action Potential in Higher Plants with Account for the Involvement of Vacuole in the Electrical Signal Generation

E. M. Novikova, V. A. Vodeneev, and V. S. Sukhov*

State University of Nizhny Novgorod, pr. Gagarina 23, Nizhny Novgorod, 603950 Russia

**e-mail: vssuh@mail.ru*

Received July 28, 2016; in final form, August 28, 2016

Abstract—Electrical signals, including action potential (AP), play an important role in plant adaptation to the changing environmental conditions. Experimental and theoretical investigations of the mechanisms of AP generation are required to understand the relationships between environmental factors and electrical activity of plants. In this work we have elaborated a mathematical model of AP generation, which takes into account the participation of vacuole in the generation of electrical response. The model describes the transporters of the plasma membrane (Ca^{2+}, Cl^-, and K^+ channels, H^+- and Ca^{2+}-ATPases, H^+/K^+ antiporter, and $2H^+/Cl^-$ symporter) and the tonoplast (Ca^{2+}, Cl^-, and K^+ channels; H^+- and Ca^{2+}-ATPases; H^+/K^+, $2H^+/Cl^-$, and $3H^+/Ca^{2+}$ antiporters), with due consideration of their regulation by second messengers (Ca^{2+} and IP_3). The apoplastic, cytoplasmic and vacuolar buffers are also described. The properties of the simulated AP are in good agreement with experimental data. The AP model describes the attenuation of electrical signal with an increase in the vacuole area and volume; this effect is related to a decrease in the Ca^{2+} spike magnitude. The electrical signal was weakly influenced by the K^+ and Cl^- content in the vacuole. It was also shown that the contribution of vacuolar IP_3-dependent Ca^{2+} channels into the generation of calcium spike during AP was insignificant with the given parameters of the model. The results provide theoretical evidence for the significance of the vacuolar area and volume in plant cell excitability.

Keywords: action potential, Ca^{2+}, higher plants, inositol-3-phosphate, simulation, vacuole

DOI: 10.1134/S1990747817010068

INTRODUCTION

Action potential (AP) is a remote electrical signal generated in response to external stimulation, in particular, light, cold, burn, pressure, touch, injury, etc. AP was revealed for the first time in the nerve and muscle cells of animals [1]. Later, the presence of AP was demonstrated in the higher [2, 3] and lower [4] plants, with the parenchymal cells of conducting bundles of the higher plants apparently having the highest excitability [5]. In contrast to animals, plants are characterized by the more negative values of resting potential and threshold potential for the generation of electrical response [5], the APs are longer (in most cases, 30–50 s and more) [6] and have no overshoot [5]. Plant APs are accompanied by considerable changes in the intra- and extracellular concentrations of Ca^{2+}, H^+, K^+, and Cl^- [5, 7, 8].

The AP triggers physiological changes including growth slowdown [9, 10], reactive oxygen species (ROS) signal initiation [9, 11], enhanced ATP level in plants [12, 13], decrease in transpiration and guttation [11, 14, 15], reduced photosynthetic activity [16–18], respiration activation [19, 20], etc. The physiological processes induced by electrical signals contribute to plant resistance to unfavorable factors and adaptation to varying environmental conditions [21–24].

The ion mechanism of AP has to be thoroughly investigated in order to understand the relationships between the effect of external stimulus and the physiological response to this stimulus. The AP mechanism of plants was suggested on the basis of experimental studies [5, 11, 25]. The first stage of the development of electrical response includes the opening of Ca^{2+} channels sensitive to various environmental factors [26–28], which leads to an increase in Ca^{2+} concentration in the cytoplasm [29]. In its turn, it activates Cl^- channels [30–32] and reduces the H^+-ATPase activity [25]. The Cl^- current depolarizes the membrane, followed by the opening of K^+ channels and subsequent repolarization. During repolarization, H^+-ATPase is activated again and the potential returns to its resting values [25, 33].

It should be noted that the described AP mechanism in the higher plants takes into consideration only the transport systems of the plasma membrane. The

involvement of vacuoles in AP generation was shown in charophytes [34–36], though such studies were not performed in the higher plants. The involvement of vacuoles in AP generation in the higher plants is favored by the following facts. (1) The vacuole occupies a considerable volume of plant cell (50–90%) [37, 38] and its shape is rather variable, which may substantially influence the area-to-volume ratio [39, 40]. One of the consequences of the large volume of the vacuole is the lesser volume of the cytoplasm; as a result, ion concentrations will change much more rapidly, which may lead to the modulation of AP parameters. (2) The vacuole is a depot of Ca^{2+} [41], which triggers AP, as well as other ions important for AP generation [8, 25, 35]. (3) The activity of transport systems of the vacuole is regulated by second messengers [42]: Ca^{2+} and IP_3, the content of which increases during AP [43, 44]. Thus, it may be supposed that the vacuole responds to the changes in composition of the cytoplasm, which cause the activation of its transport systems, i.e., the vacuole can play a key role in signaling and ion homeostasis maintenance.

However, experimental studies of the role of vacuoles in AP generation in the higher plants are difficult to perform because of small cell size. This problem can be solved through the mathematical modeling of AP in the higher plants. There are a number of models describing the involvement of ion transport systems of the plasma membrane in the generation of electrical response in plants [45–51]. In addition, some models describe the involvement of intracellular depots in the regulation of Ca^{2+} and electrical activity [43, 44]. Thus, the mathematical models presented in scientific literature cannot be used for theoretical analysis of the role of vacuole in electrogenesis of the higher plants.

This work was aimed at the development of a mathematical model of AP taking into account the ion transport systems of the plasma membrane and the tonoplast and theoretical analysis of the role of vacuole in AP generation in the higher plants.

MATHEMATICAL DESCRIPTION OF THE MODEL

The model is based on the scheme of transport processes in the plasma membrane and the tonoplast, which is shown in Figure 1. For simplicity, it was assumed that the excited cells had a spherical shape.

The relationship between the changes in the membrane potential and the ion channels is described by the following equation [45, 52]:

$$\frac{dE_m}{dt} = \frac{1}{C} F \Sigma z_r j_r, \quad (1)$$

where E_m is the membrane potential, C is the membrane capacity, F is the Faraday's constant, j_r is the ion r flow, z_r is the ion r charge. Potential difference on the plasma membrane was calculated with the value of electric potential in the apoplast taken as zero. In plants, the systems of both passive and active transport play the key role in the maintenance of membrane resting potential and AP generation [5, 25], which is taken into account in the model.

The passive transport is described by the Goldman–Hodgkin–Katz equation [48, 50]. At the same time, it is known that the activity of ion channels is regulated by the ratio of concentrations of the transported ion on both sides of the membrane [53, 54]. The widely known three-barrier model of ion channel [55, 56] can be used to describe this dependence. We have described the effect of channel saturation. Here, the probabilities that the ion will be linked to the channels at the inner (θ_{in}) and outer (θ_{out}) side are described by the equations

$$\theta_{in} = \frac{c_{in}}{c_{in} + \gamma}, \quad \theta_2 = \frac{c_{out}}{c_{out} + \gamma}, \quad (2)$$

where c_{in} and c_{out} are the ion concentrations on both sides of the membrane (subscripts in and out refer to the cytoplasm and the apoplast (or vacuolar contents), respectively); $\gamma = \frac{k_2}{k_1}$ is the channel–ion complex dissociation constant, where k_1 is the rate constant for ion binding with the channel site and k_2 is the rate constant for disintegration of the channel–ion complex (for simplicity, it was accepted that these constants are the same on both sides of the channel).

The probabilities that the ion will not be linked to the respective sites of the channel, η_{in} and η_{out}:

$$\eta_{in} = 1 - \theta_{in} = \frac{\gamma}{\gamma + c_{in}}, \quad \eta_{out} = 1 - \theta_{out} = \frac{\gamma}{\gamma + c_{out}}. \quad (3)$$

It is assumed that the probability of ion passage through the channel is determined by the product of probabilities $\theta_{in}\eta_{out}$ for the outward flow and $\theta_{out}\eta_{in}$ for the inward flow. Final Eq. (4) for the passive flow through the channels was used henceforth:

$$J = zuP'_{max}p_o \frac{(\theta_{in}\eta_{out} - \theta_{out}\eta_{in1}\exp(-zu))}{1 - \exp(-zu)}, \quad (4)$$

where p_o is the ion channel open-state probability, $P'_{max} = P_{max}c_{chan}$ is the maximum permeability per unit of area, P_{max} is the maximum permeability of the ion channel, c_{chan} is the concentration of channels per unit of area, z is the ion charge, $u = \frac{E_m F}{RT}$ is normalized dimensionless potential, R is the gas constant, and T is the absolute temperature.

The model takes into account the regulation of channels by membrane potential and the presence of ligands. There are charged groups within the channel. They can be differently positioned depending on the potential, thereby determining the channel activity. Different states of channels (closed (c), open (o) and

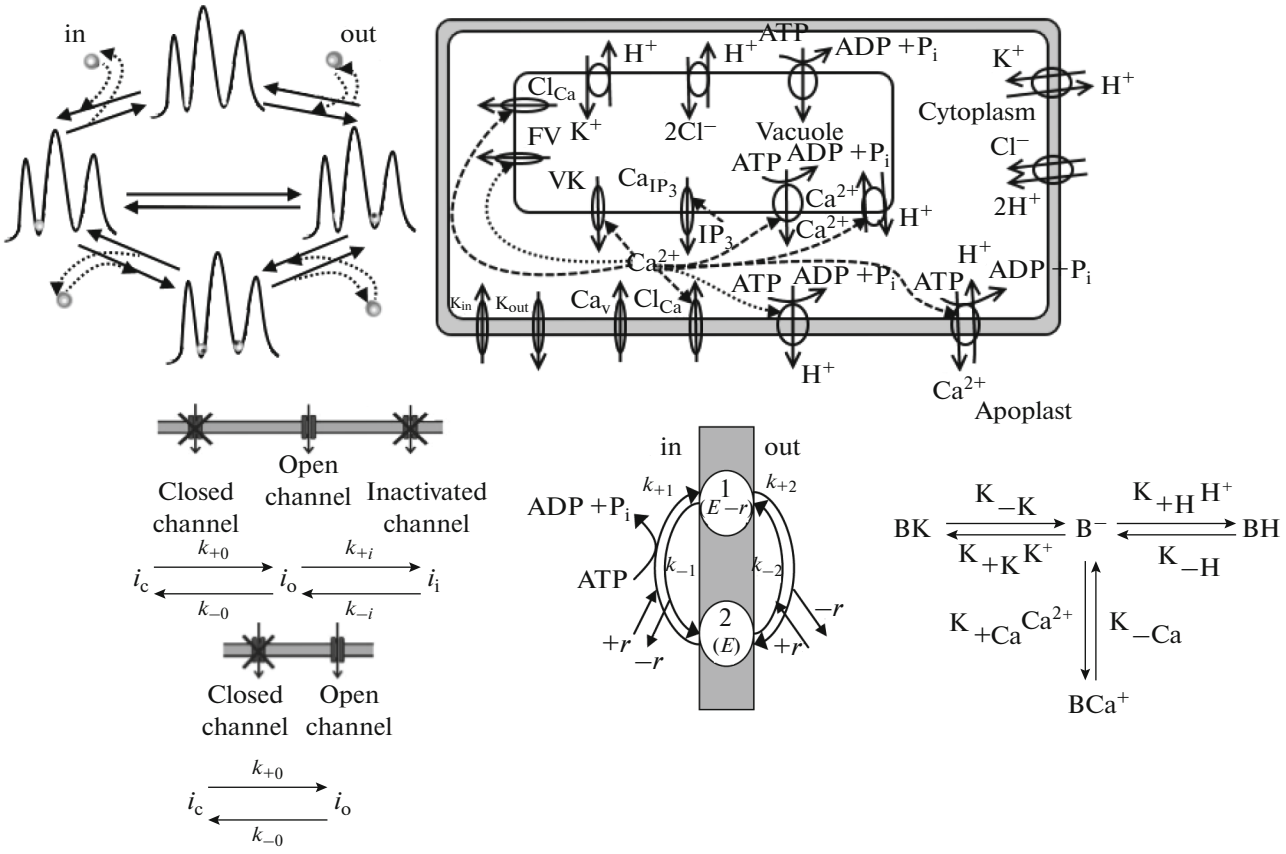

Fig. 1. The model of electrogenesis in higher plants. Scheme at the top right corner presents transport systems and their regulation by Ca^{2+} and IP_3. *Dashed* and *dotted lines* show activation by second messengers and inactivation, respectively. Scheme at the top left corner is a three-barrier model of a channel; transitions between different states of the channel are shown: i_c, closed; i_o, open; i_i, inactivated. At the bottom right corner, a "two-state" model used to describe ATPases and the buffer system of the apoplast are presented.

inactivated (i)) are separated by potential barriers. The barrier crossing rates are determined by interactions between the ions with charged groups in the membrane and their averaged charges (c_o and c_i). The rate constants for channel transitions between different states can be represented by the modified Arrhenius equation [48, 50]:

$$k_{+o(+i)} = k_{o(i)} \exp\left(\frac{uc_{o(i)}}{2}\right),$$
$$k_{-o(-i)} = k_{o(i)} \exp\left(u_{o(i)}c_{o(i)} - \frac{uc_{o(i)}}{2}\right), \quad (5)$$

where k_{+o} and k_{-o} are the rate constants for transition from the closed to open state and back, k_{+i} and k_{-i} are the rate constants for transition from the open to inactivated state and back, u_o and u_i are the normalized potential barriers for transition of the channels from the close to open state and from the open to inactivated state, respectively, k_o and k_i are the rate constants for transition of the channel between the closed and open states and between the open and inactivated states, with u, u_o, u_i being equal to zero.

The probabilities of opening for the most of channels are described by a model taking into account only two states of the channel (open (p_o) and closed (p_c), Eq. (6)); for calcium channel, it is a model with three states (closed, open, inactivated (p_i), Eq. (7)) [50]:

$$\frac{dp_o}{dt} = k_{+o}(1 - p_o) - k_{-o}p_o, \quad (6)$$

$$\frac{dp_o}{dt} = k_{+o}(1 - p_o - p_i) - k_{-o}p_o - k_{+i}p_o + k_{-i}p,$$
$$\frac{dp_i}{dt} = k_{+i}p_o - k_{-i}p_i. \quad (7)$$

At the same time, only two approaches are used to describe the probability of ion channel opening. For "slow" channels (i.e., the channels with activation times comparable to or exceeding the time of AP generation, the Ca_v and K_{out} channels in the model), differential Eqs. (6) and (7) were solved numerically. For "fast" channels (i.e., the channels with activation

times much less than the time of AP generation, the K_{in}, Cl_{Ca}, FV, VK, and Ca_{IP3} channels in the model), it was considered that the equilibrium state was achieved instantaneously (the stationary solution of Eq. (6)):

$$p_o = \frac{1}{1+\exp\left(kc_o\left(u_o-u\right)\right)}. \quad (8)$$

As was mentioned previously, Ca^{2+} and IP_3 regulate the function of most of the passive and active transport systems of the plasma membrane and the tonoplast (Fig. 1). The ligand binding is a probabilistic process depending on ligand concentration ([L]), affinity to the channel (reflected in the concentration for half-activation, K), and the number of bound ligand molecules (the Hill coefficient, n). The probability of channel opening with the activator ligand concentration in the medium [L]:

$$P_o = \frac{[L]^n}{[L]^n + K^n}. \quad (9)$$

The probability that the channel will remain open at the inactivating ligand concentration in the medium [L]:

$$P_o = \frac{K^n}{[L]^n + K^n}. \quad (10)$$

In a state of rest, the concentration of calcium in the cytoplasm is low [41]; it penetrates into cells from the environment during depolarization of the plasma membrane. On appearance of an external stimulus, in particular, during depolarization, the enzymes of the cascade of IP_3 synthesis are activated, probably due to local penetration of calcium ions and activation of phospholipase C [57, 58]. When describing the IP_3 dynamics, we relied on the works [44, 58] where it was described depending on the intensity of current through the plasma membrane in Chara. Based on the experimental data [59], in our model we also added a component to take into account the synthesis of IP_3 in a state of rest, at the background level (the third summand in Eq. (11)):

$$\frac{d[IP_3]}{dt} = k_4 f(i) i - k_{-4}[IP_3] + J_{synthesis}, \quad (11)$$

where $f(i) = 1 - \frac{i_0}{i}$ is the function describing the dependence of IP_3 on the input current, i_0 is the minimum current through the plasma membrane when IP_3 synthesis begins, i is the input current through the plasma membrane, with $\frac{i}{i_0} > 1$ for the induction of additional IP_3 synthesis or $\frac{i}{i_0} < 1$ for IP_3 synthesis at the background level, and $f(i) = 0$, k_4 is the rate constant for IP_3 synthesis, k_{-4} is the rate constant for IP_3 decomposition, $J_{synthesis}$ is the rate of IP_3 synthesis at the background level, with $J_{synthesis} = k_{-4}[IP_3]_{stat}$, $[IP_3]_{stat}$ is the background concentration level.

The primary active transport (H^+-ATPase and Ca^{2+}-ATPase) is described by using a model for the two states of the pump: with and without the ion. The model not only describes the dependence on ion gradients and the voltage across the membrane but also the effect of saturation. The stationary flows through ATPases [60]:

$$j_p = E_o \frac{k_{+1}k_{+2} - k_{-1}k_{-2}}{k_{+1} + k_{+2} + k_{-1} + k_{-2}}, \quad (12)$$

where E_o is the total ATPase concentration in the membrane, k_{+1} is the rate constant for ATPase binding with the ion at the inner side of the membrane, k_{-1} is the rate constant for disintegration of the ion–ATPase complex without ion transfer across the membrane, k_{+2} is the rate constant for disintegration of the ion–ATPase complex with ion transfer across the membrane, k_{-2} is the rate constant for ATPase binding with the ion at the outer side of the membrane. Indices (1) and (2) are used to denote the potential-independent and potential-dependent rate constants, respectively. The rate constants are described as follows [50, 61]:

$$k_{+1} = k_1[I_1]_{in}, \quad k_{-1} = k_1 \exp\left(\frac{-\Delta G_{ATP}}{RT}\right),$$
$$k_{+2} = k_2 u \frac{1}{1-\exp(-u)}, \quad (13.1)$$
$$k_{-2} = k_2[I_1]_{out} u \frac{\exp(-u)}{1-\exp(-u)},$$

$$k_{+1} = k_1[I_1]_{in}[I_2]_{out}, \quad k_{-1} = k_1 \exp\left(\frac{-\Delta G_{ATP}}{RT}\right),$$
$$k_{+2} = k_2 u \frac{1}{1-\exp(-u)}, \quad (13.2)$$
$$k_{-2} = k_2[I_1]_{out}[I_2]_{in} u \frac{\exp(-u)}{1-\exp(-u)},$$

where k_1 and k_2 are the rate constants at $u = 0$, ΔG_{ATP} is the energy of ATP hydrolysis, ATPases transfer one type of ions, [I_1], (13.1) or, when functioning as antiporters, two types of ions, [I_1] and [I_2] (13.2).

Secondary active transport is described as a difference between the input and output ion flows. Its activity is determined by membrane potential but it is described by the modified Goldman–Hodgkin–Katz equation [50]. The ion transport via antiport and symport is described by Eq. (14.1) and Eq. (14.2), respectively:

$$j = \frac{Ezu}{1-\exp(-zu)} \times \left([A]^n_{in}[B]^m_{out} - [A]^n_{out}[B]^m_{in}\exp(-zu)\right), \quad (14.1)$$

$$j = \frac{Ezu}{1-\exp(-zu)} \times \left([A]_{in}^{n}[B]_{in}^{m} - [A]_{out}^{n}[B]_{out}^{m}\exp(-zu)\right), \quad (14.2)$$

where n and m are the numbers of transported ions A and B per working cycle of the transporter, E is the product of transporter concentration and rate constant at $u = 0$ and 1 M concentration of the transported ions at both sides of the membrane.

The electrically neutral transport is described by the modified Fick's equation; the ion transport via antiport is described by Eq. (15) [50]:

$$j = E\left([A]_{in}[B]_{out}^{m} - [A]_{out}^{n}[B]_{in}^{m}\right). \quad (15)$$

The regulation of active transport systems by ligands is described similar to the ion channels. The operating speed of active transport systems also depends on the ambient temperature. The Q_{10} coefficient is introduced to describe temperature sensitivity like in the previous work [50].

The competitive binding of apoplastic buffer with the Ca^{2+}, K^+, and H^+ ions is described by the Gradmann's model ([49], see Fig. 1 for the buffer scheme). At the same time, the dynamics of ion association/dissociation is described by the following equations:

$$\frac{d[r]}{dt} = k_{-r}([r_\Sigma] - [r]) - k_{+r}([B_\Sigma] - [Ca_\Sigma] - [K_\Sigma] - [H_\Sigma] + [Ca] + [K] + [H])[r], \quad (16)$$

where r is one of the ions that can be bound by the buffer (Ca^{2+}, K^+, or H^+), $[r]$ and $[r_\Sigma]$ are its free and total concentrations, respectively, k_{-r} and k_{+r} are the rate constants for dissociation and association of the r ion and buffer complex with the total concentration $[B_\Sigma]$, respectively, $[K_\Sigma]$ is the total potassium concentration, $[H_\Sigma]$ is the total proton concentration, $[Ca_\Sigma]$ is the total calcium concentration. For calcium, a simplification has been made: one charged group of the apoplast binds one calcium ion.

The curves of pH dependence on the total $[H^+]$ concentration in the cytoplasm and in the vacuolar contents have been plotted on the basis of experimental data [62] and are described by the following equation:

$$d\mathrm{pH} = \frac{d\left[H^+\right]}{C}, \quad (17)$$

where C is the buffer capacity, dpH is the pH change after the entry/release of protons.

Calmodulin, being a calcium buffer, plays a key role in maintaining cytoplasmic free calcium [63]. Calmodulin has two ends, each of them successively binding two calcium ions [64]. The dependence of free calcium concentration ($[Ca^{2+}]$) on its total concentration (bound + free, $[Ca_\Sigma]$) was revealed on the basis of the model proposed in [64]. To simplify the solution, such dependence is described by regression Eq. (18) (the coefficient of determination, 0.999), which is further used to describe the buffer properties of the cytoplasm for calcium:

$$[Ca^{2+}] = 0.2425[Ca_\Sigma]^{0.862}, \quad (18)$$

where coefficient 0.2425 and degree 0.862 were obtained with approximation. In Eq. (18) calcium concentration is expressed in μmols.

The vacuole has a high calcium concentration [41] and strong buffer properties determined by the high content of compounds capable of binding Ca^{2+}, including malates, phosphates, chlorides, carbonates and nitrates, as well as the vacuolar Ca^{2+}-binding proteins [65–67]. Therefore, it is assumed that the concentration of calcium ions in the vacuole is constant.

The model was solved numerically by the Euler's method. The parameters and initial conditions for equations of the model were obtained on the basis of the published data (Table 1).

RESULTS AND DISCUSSION

At the first step of the research, the model was verified by simulating AP generation in response to cooling. The results (Fig. 2, Table 2) show that the simulated signal is in good agreement with experimental responses, in particular, has the basic properties of AP [86–88]: the threshold potential ($E_{m\,threshold}$) and temperature threshold ($T_{threshold}$), above which the AP develops according to the all-or-none principle, depolarization and subsequent repolarization, etc. Thus, the model showed a good correspondence with experimental data and can be used for further analysis.

It is known that the volume and area of the vacuole are highly variable and can change depending on the functional state of a cell [39, 40]. Hereinafter, we investigated the effects of these parameters on the ability of cells to generate electrical response.

The influence of vacuole volume on AP generation by plant cells was studied assuming that the vacuole has a constant area to volume ratio and a spherical shape. The signals simulated by the model are pre-

Table 1. Parameters of transport and buffer systems and initial conditions for numerical solution of the mathematical model

Plasmalemma			Tonoplast		
parameter	value	reference	parameter	value	reference
Cl_{Ca} channels			FV channels		
$P_{max}c_{chan}$	1×10^{-6} M cm s^{-1}	Accepted	$P_{max}c_{chan}$	1×10^{-7} M cm s^{-1}	[74]
c_o	3.1	[68]	c_o	0.55	
u_o	−4.91	[68]	u_o	−2.72	
γ	0.054 M	[69]	γ	0.27 M	
K	8×10^{-6} M	[50]	K	6.3×10^{-6} M	
n	2	[70]	n	0.7	
K_{out} channels			VK (TPK1) channels		
$P_{max}c_{chan}$	1.21×10^{-6} M cm s^{-1}	Accepted	$P_{max}c_{chan}$	2×10^{-6} M cm s^{-1}	[75]
c_o	1.13	[50]	p_o	0.6	
u_o	−2.53	[50]	γ	3.1 M	
k_o	0.5 s^{-1}	[50]	K	7.5×10^{-6} M	
γ	3.5×10^{-3} M	Accepted	n	1	
K_{in} channels			Ca_{IP3} channels		
$P_{max}c_{chan}$	1.21×10^{-6} M cm s^{-1}	[53]	$P_{max}c_{chan}$	7×10^{-9} M cm s^{-1}	[76]
c_o	2.7	[71]	γ	0.4 M	
u_o	−6.39	[71]	K	2.2×10^{-7} M	
γ	3.5×10^{-3} M	[53]	n	1	
Ca_v channels			Cl_{Ca} channels		
$P_{max}c_{chan}$	2.5×10^{-10} M cm s^{-1}	[72]	$P_{max}c_{chan}$	1×10^{-6} M cm s^{-1}	[77]
c_o	1.15	[50]	c_o	2	[78]
u_o	−3.51	[50]	u_o	−1.68	[78]
c_i	1.28	[50]	γ	0.00144 M	[77]
u_i	−7.01	[50]	K	1×10^{-6} M	[72]
γ	9.9×10^{-5} M	[54]	n	1	[72]
K^+/H^+ antiport			K^+/H^+ antiport		
V_K	0.015 M^{-1} s^{-1}	[50]	V_K	2.23×10^{-3} M^{-1} s^{-1}	Accepted
$2H^+/Cl^-$ symport			$H^+/2Cl^-$ antiport		
V_{Cl}	3.12 M^{-2} s^{-1}	Accepted	V_{Cl}	0.028 M^{-3} s^{-1}	[72]
H^+-ATPase			$Ca^{2+}/3H^+$ antiport		
E_0	0.15 M	Accepted	V_{Ca}	9.4×10^{10} M^{-4} s^{-1}	[72]
k_1	0.45 s^{-1}	[50]	K	1.5×10^{-5} M	
k_2	2.58×10^{-4} s^{-1}	[50]	n	1	
K	4×10^{-7} M	[50, 73]	H^+-ATPaze		
n	2	[73]	E_0	0.25 M	[72]
Stoichiometry	$1H^+$:1 ATP	[72]	k_1	850000 s^{-1}	[79]
			k_2	0.09 s^{-1}	[79]
			Stoichiometry	2 H^+:1 ATP	[80]

Table 1. (Contd.)

Plasmalemma			Tonoplast		
parameter	value	reference	parameter	value	reference
Ca^{2+}-ATPaze			Ca^{2+}-ATPaze		
E_0	3.23 M	Accepted	E_0	0.0083 M	[72]
k_1	45 s^{-1}	[50]	k_1	0.12 s^{-1}	[72]
k_2	2.58×10^{-5} s^{-1}	[50]	k_2	2.92×10^{-7} s^{-1}	[72, 81]
K	5×10^{-7} M	[72]	K	7×10^{-6} M	[81]
n	2	[72]	n	1	[38, 82]
Stoichiometry	$1Ca^{2+}$, $1H^+$:1 ATP	[50]	Stoichiometry	$1Ca^{2+}$:1 ATP	[82]
Cell characteristics					
C	10^{-6} F sm^{-2}	[35]	Q_{10}	3	[50]
E_m (plasma membrane)	−170 mV	[5]	E_m (tonoplast)	−40 mV	[5]
S_{cell}/V_{cell}	10^4 cm^{-1}	[50]	R_{cell}	0.0003 cm	[50]
V_{ap}/V_{cell}	0.1	[49]	V_{vac}/V_{cell}	0.5–0.8	[72, 82]
k_4	21.5 M^{-1} $cells^{-1}$	[44]	k_{-4}	0.2 s^{-1}	[44]
i_0	1×10^{-6} A	Accepted	$[IP_3]_{stat}$	4.76×10^{-8} M	[59]

Initial ion concentrations and buffer properties			
	Apoplast	Cytoplasm	Vacuole
$[K^+]_0$	3.5×10^{-3} M [50]	0.16 M [5, 50]	0.67 M [84]
$[Cl^-]_0$	2.7×10^{-3} M [50]	0.02 [5]	0.07 M [72]
$[Ca^{2+}]_0$	3.3×10^{-4} M [41]	10^{-7} M [74]	5×10^{-3} M [41], accepted as a constant
pH_0	6.0 [50]	7.2 [83]	5.8 [85]
	$[K_\Sigma]_0 = 0.188$ M, $[H_\Sigma]_0 = 0.0089$ M, $[Ca_\Sigma]_0 = 0.002$ M (accepted) $[B] = 0.2$ M, $K_H = 10^{-6}$ M, $K_{Ca} = 10^{-3}$ M, $K_K = 10^{-4}$ M [50]	$C_{cyt} = 0.02825$ M pH^{-1} [62] $[Ca_\Sigma]_0 = 3.6 \times 10^{-7}$ M (accepted on the basis of Eq. (18) and $[Ca^{2+}]_0 = 10^{-7}$ M)	$C_{vac} =$ 0.02874 M pH^{-1} [62]

sented in Figure 3. It has been shown that the amplitude of AP and value of the maximum change in ionized calcium ($\Delta[Ca^{2+}]$) concentration decrease to certain values as the relative volume of the vacuole increases and hereafter change insignificantly (Figs. 4a, 4b). It can be accounted for by the fact that the increase in vacuole volume and area leads to an increase in the number of Ca^{2+}-ATPases and $Ca^{2+}/3H^+$ antiporters activated by Ca^{2+}, which enhances its transport into the vacuole. As a consequence, more substantial cooling is needed to reach the threshold $[Ca^{2+}]$ value that triggers AP. This mechanism is confirmed by the higher temperature threshold as a result of increase in the vacuole volume (Fig. 4c).

During AP, only a slight electrical response (below 10 mV) including depolarization followed by hyperpolarization is observed on the tonoplast, and the threshold of response generation and slowdown increases along with the increase in vacuole volume (Fig. 3b). According to the data obtained for Chara [34, 35], both depolarization and hyperpolarization can be observed on the tonoplast depending on the cytoplasmic to vacuolar ion content ratio. The responses are characterized by large amplitudes (tens of millivolts) and are apparently determined by the Ca^{2+}, Cl^-, and

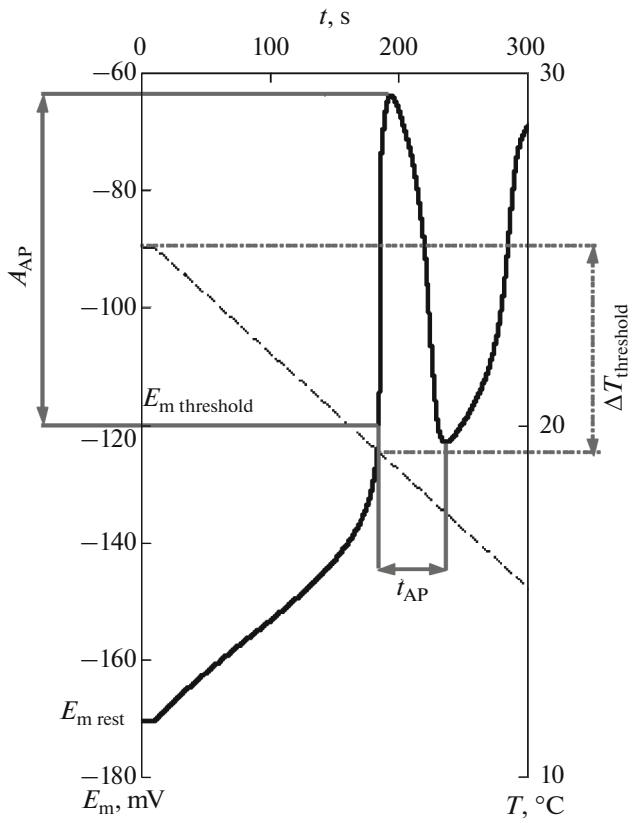

Fig. 2. Action potential simulated by the model. *Black solid line* shows a change in the potential on the plasma membrane during AP; *black dashed line* shows a temperature change. A_{AP}, AP amplitude; t_{AP}, AP duration; $E_{m\ rest}$, resting potential; $E_{m\ threshold}$, threshold potential, at which AP generation begins; $\Delta T_{threshold}$, temperature change necessary for the AP induction. The potential difference across the plasma membrane was calculated at the value of electric potential in the apoplast set to zero.

K^+ flows [34]. It may be supposed that the mechanism of electrical response on the tonoplast in higher plants is also associated with the Ca^{2+} flow activating the potassium and chloride channels of the vacuole. At the same time, the low magnitude of response in higher plants is probably accounted for by their specific vacuolar to cytoplasmic ion ratios. The essential role of Ca^{2+} in the formation of response on the tonoplast is also confirmed by the slowdown of its development at a decrease in the calcium spike.

The vacuole has a variable shape [39, 40] and, hence, the total area of the tonoplast within a cell can change irrespective of the total volume. Hence, we have analyzed the effect of the area of the vacuole on AP generation with its unchanged relative volume taken equal to 0.7 (Fig. 5). In this case, the increase in vacuole area is accompanied by a decrease in the amplitude of electrical response on the plasma membrane and the tonoplast and $\Delta[Ca^{2+}]$ until disappearance, as well as by an increase in the temperature

Table 2. Comparison of the main characteristics of action potential on the plasmalemma simulated by the model and obtained experimentally

AP characteristic	Signal simulated by the model	Experimental data
A_{AP}, mV	70	40–120 [31, 33, 87, 88]
t_{AP}, s	52	11–285 [25, 31, 33]
$\Delta T_{threshold}$, °C	5.8	3.8–8.8 [87, 89]
$E_{m\ rest}$ (plasmalemma), mV	−170	−190...−140 [25, 33]
$E_{m\ threshold}$ (plasmalemma), mV	−120	−120 [25]
Maximum rate of repolarization, $mV\,s^{-1}$	3.5	0.5–3.7 [33]

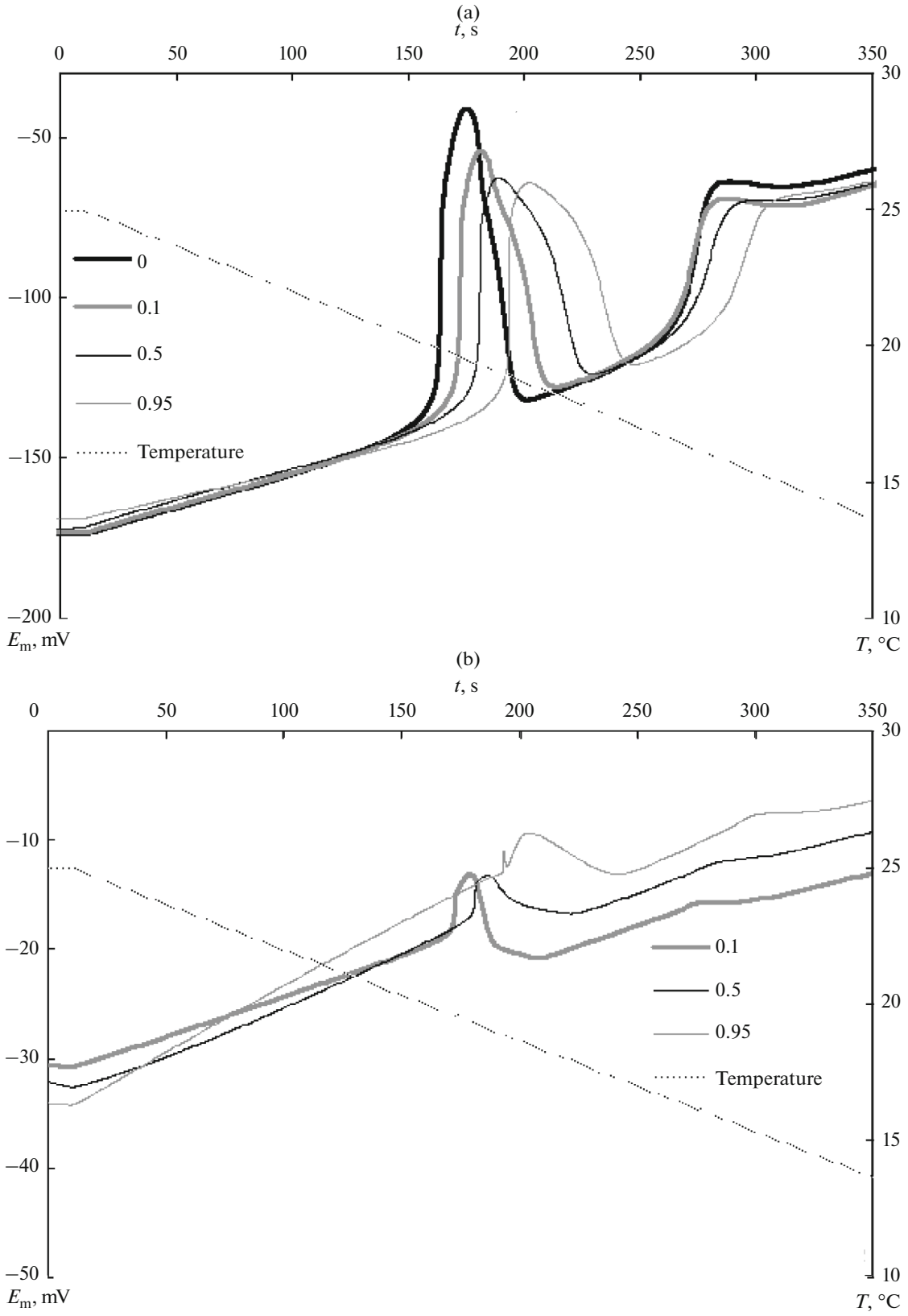

Fig. 3. Action potentials simulated by the model with varying relative volumes of the vacuole: (a) signal developing on the plasma membrane; (b) signal developing on the tonoplast. Values of the relative volume are presented in the captions to the lines; zero value corresponds to the AP simulated by the model without vacuole. The potential difference across the plasma membrane was calculated at the value of electric potential in the apoplast set to zero; for calculations of the potential difference on the tonoplast, the potential within the vacuole was set to zero.

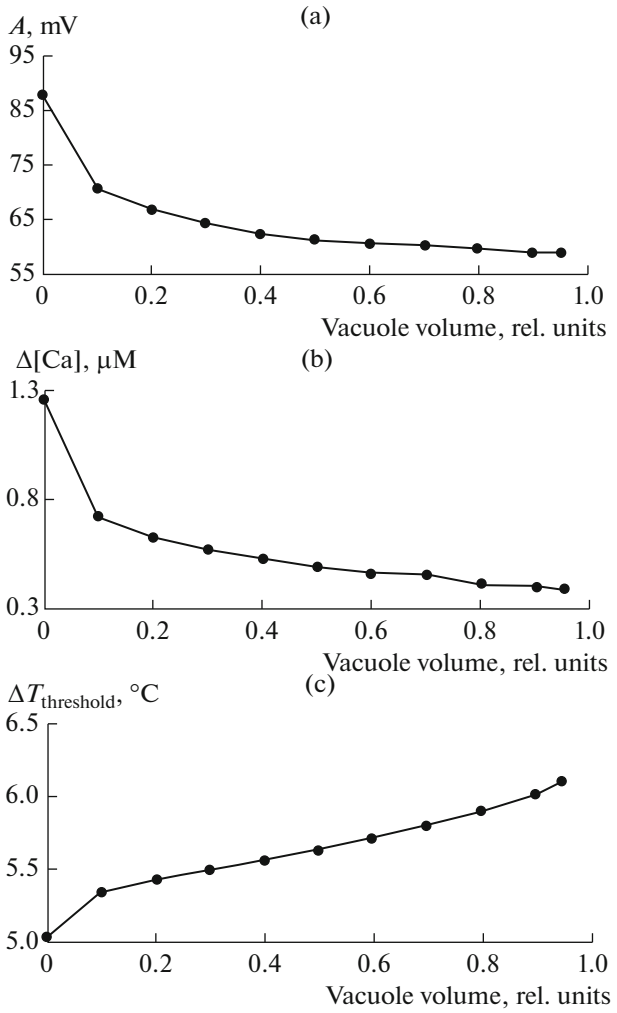

Fig. 4. The influence of the vacuole volume on the parameters of action potential and Ca^{2+} spike. (a) Dependence of the AP amplitude on the relative volume of vacuole; (b) dependence of the calcium signal amplitude on the relative volume of the vacuole; (c) dependence of the temperature threshold of the AP generation on the vacuole relative volume.

threshold (Fig. 6). Like in case of increasing vacuole volume, the mechanism of signal attenuation with increasing area is probably associated with the increased number of Ca^{2+}-ATPases and $Ca^{2+}/3H^+$ antiporters in the cell. The similarity of mechanisms is confirmed by the similar curves of the AP amplitude dependence on $\Delta[Ca^{2+}]$ with increasing area or volume (Fig. 7).

In addition to geometric characteristics, AP can be potentially influenced by the concentrations of vacuolar ions forming the potential. In particular, it is known that potassium and chloride concentrations may vary within a very broad range [72]. Hence, we investigated the effects of different initial concentrations of vacuolar potassium and chloride on the development of electric reactions during cell cooling (Fig. 8). As Figure 8a shows, the decrease in the initial concentration of vacuolar potassium does not lead to substantial changes in AP characteristics but only a slight decrease in response generation threshold. At the same time, a more negative resting potential is set on the tonoplast (Fig. 8b), probably due to the negative shift in potassium equilibrium potential when the content of potassium in the vacuole decreases. It also increases the thresholds for the development of electrical response on the tonoplast. When the initial chloride concentration in the vacuole is changed, the differences in AP are actually absent (Fig. 8c). The increase in the initial chloride concentration leads to a slight hyperpolarization of the tonoplast (Fig. 8d) and insignificant increase in the thresholds for electrical response development on the tonoplast. Thus, the change in the initial vacuolar content of potassium and chloride has a weak effect on the development of electrical responses during cell cooling.

Since the vacuole can be a source of calcium under the conditions of electrical response development [35, 41], hereinafter we analyzed the role of IP_3-sensitive

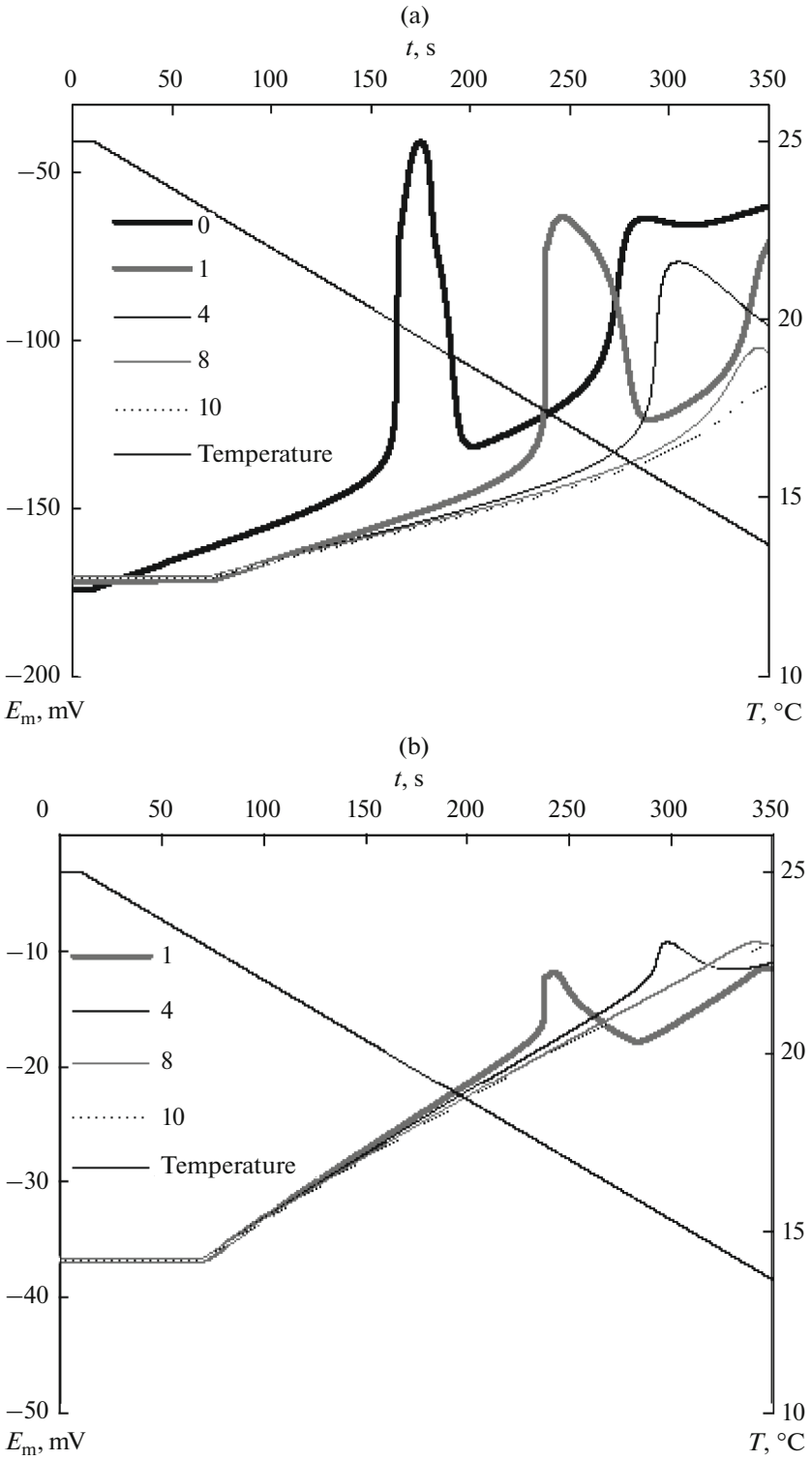

Fig. 5. Action potential simulated by the model with varying area and constant volume of the vacuole (0.7): (a) the signal developing on the plasma membrane; (b) the signal developing on the tonoplast. Zero value corresponds to the AP simulated by the model without the vacuole; value 1 corresponds to the AP used for verification of the model; other values demonstrate multiple increases in the area compared to its value for the variant used for verification. The potential difference across the plasma membrane was calculated at the value of electric potential in the apoplast set to zero; the potential difference on the tonoplast was calculated at the value of potential within the vacuole set to zero.

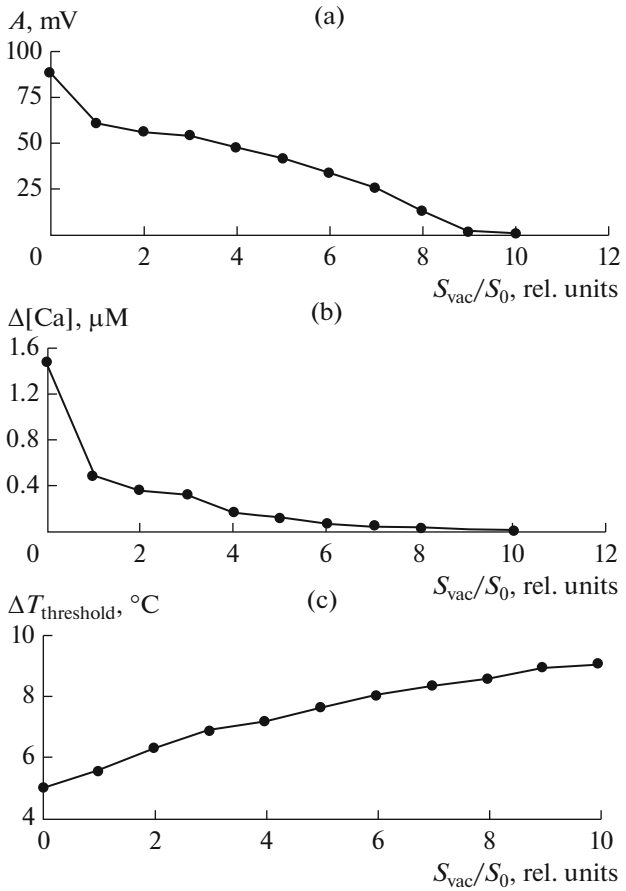

Fig. 6. The influence of the vacuole area on the parameters of action potential and Ca^{2+} spike. (a) Dependence of the AP amplitude on the relative area of the vacuole (S_{vac}/S_0); (b) dependence of the calcium signal amplitude on S_{vac}/S_0; (c) dependence of the temperature threshold of the AP generation on S_{vac}/S_0.

vacuolar Ca^{2+} channels in the formation of Ca^{2+} spike during AP. The model simulates the increase in the Ca^{2+} flow through these channels in the depolarization phase and its decrease to a certain minimal stationary value in the repolarization phase (Fig. 9a). The

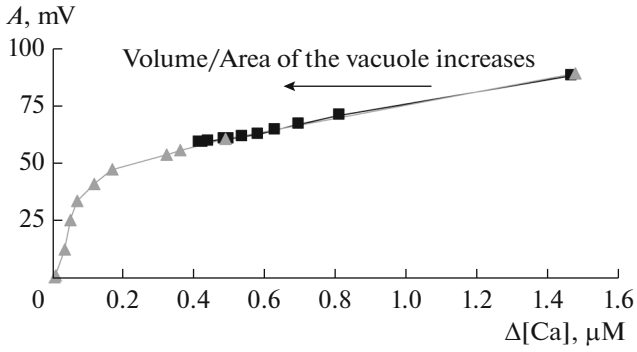

Fig. 7. Dependence of the action potential amplitude on calcium peak amplitude with increasing vacuole relative volume (*black*) and with increasing vacuole area at a constant volume (*gray*). Respective values were taken from Figs. 4 and 6.

cells having all transport systems of the plasma membrane and the vacuole were used as a control; the current through IP_3 receptors was only background and did not change after excitation (Fig. 9b). With the inclusion of a component dependent on the value of depolarization current through the plasma membrane, the Ca^{2+} peak in the cytoplasm increases; however, this increase is small compared to the control: about 30% of the control (Fig. 9c). At the same time, the parameters of AP with IP_3 involved in the regulation of calcium concentration are not substantially different from the parameters without IP_3 (Fig. 9b).

Thus, the vacuole most likely does not make any considerable contribution to the Ca^{2+} spike formation during AP in the higher plants, at least, when using the permeability values for IP_3 receptors obtained in the experiments with sugar beet [76]. However, it cannot be excluded that they have different permeability to other objects; at a higher permeability of IP_3 receptors, the contribution of the vacuole may be more significant.

The theoretical analysis of the role of vacuole in the mechanism of AP generation demonstrates its poten-

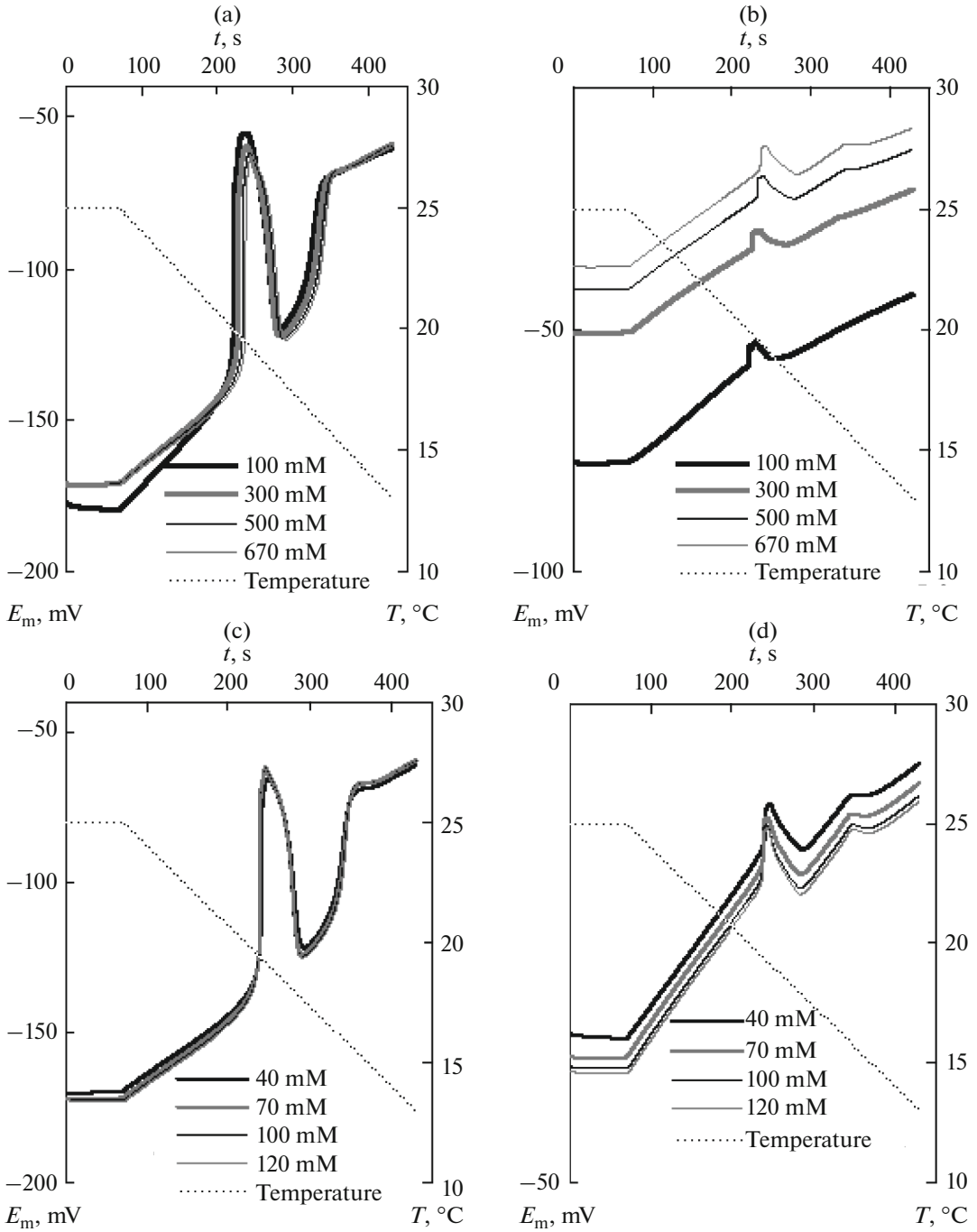

Fig. 8. The influence of the initial concentrations of potassium and chloride ions in the vacuole on the development of electrical responses on the plasma membrane and the tonoplast. The cooling-induced change in potential (a) on the plasma membrane and the tonoplast (b) at different initial potassium concentrations in the vacuole. The cooling-induced change in potential (c) on the plasma membrane and the tonoplast (d) at different initial chloride concentrations in the vacuole. The concentrations are given in the legends. The potential difference across the plasma membrane was calculated at the value of electric potential in the apoplast set to zero; for calculations of the potential difference on the tonoplast, the potential within the vacuole was set to zero.

tial involvement in the regulation of electrical response value with the changing vacuolar area and volume. The concentrations of potassium and chloride ions in the vacuole weakly influence the action potential; the contribution of IP_3-sensitive Ca^{2+} channels to the calcium spike formation during AP is minor too. The result shows that the role of vacuole in AP formation in the higher plants is associated with the consumption of calcium entering the cell by the active transport systems of the tonoplast rather than with Ca^{2+} release from the vacuole through the channels during AP generation. Thus, one of the functions of the vacuole is probably to

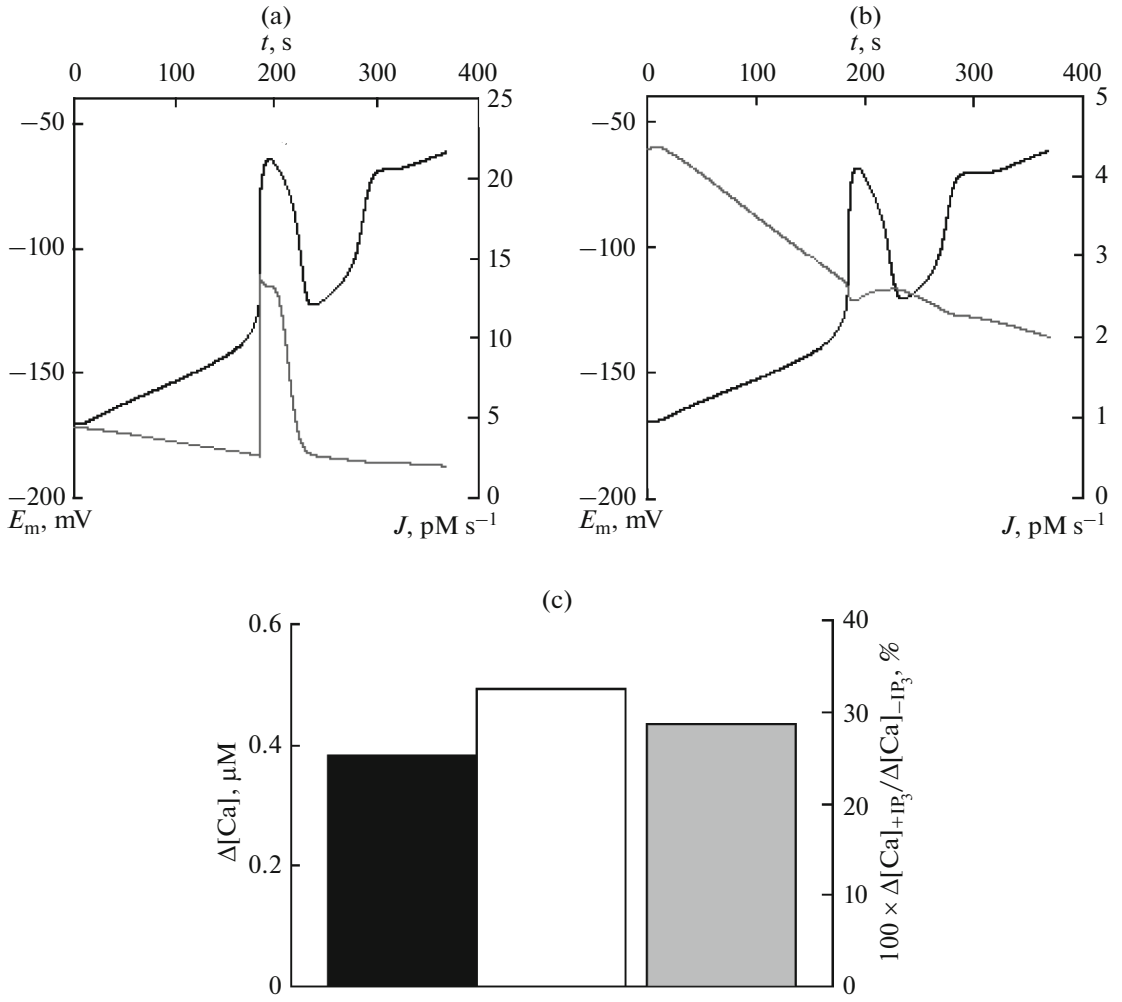

Fig. 9. The involvement of IP_3-sensitive Ca^{2+} channels in the generation of AP and Ca^{2+} spike. (a) Ca^{2+} flow through the IP_3-dependent Ca^{2+} channels and membrane potential changes during AP; (b) Ca^{2+} flow through the IP_3-dependent Ca^{2+} channels and the change in membrane potential during AP in the absence of the IP_3 content changes; (c) absolute values of calcium spike during AP with varied (*white column*) and unchanged (*black column*) content of IP_3, as well as relative contributions of the IP_3-dependent Ca^{2+} channels to the calcium spike generation during AP (*gray column*).

maintain the relatively low concentration of calcium ions in the cytoplasm under excitation. In general, the analysis shows the importance of changes in the parameters of the vacuole for AP modulation in different plant tissues and organs, which may be significant for response in general. The results can explain, in particular, the age-related change in cell excitability [5, 90] probably associated with the changes in vacuole area and shape during plant growth and development.

ACKNOWLEDGMENTS

The work was supported by the Russian Science Foundation (project no. 14-26-00098).

REFERENCES

1. Martonosi A.N. 2000. Animal electricity, Ca^{2+} and muscle contraction. A brief history of muscle research. *Acta Biochim. Pol.* **47**, 493–516.
2. Burdon-Sanderson J. 1873. Note on the electrical phenomena which accompany stimulation of the leaf of *Dionaea muscipula*. *Philos. Proc. R. Soc. Lond.* **21**, 495–496.
3. Bose J.C. 1926. *The nervous mechanism of plant.* London: Longmans, Green et Co.
4. Trebacz K., Zawadzki T. 1985. Light-triggered action potentials in the liverwort *Conocephalum conicum*. *Physiol. Plant.* **64**, 482–486.
5. Opritov V.A., Pyatygin S.S., Retivin V.G. 1991. *Bioelektrogenez u vysshikh rasteniy* (Bioelectrogenesis in Higher Plants), Moscow: Nauka.

6. Stahlberg R., Cleland R.E., Volkenburgh E. 2006. Slow wave potentials – a propagating electrical signal unique to higher plants. In: *Communication in Plants*. Baluška F., Mancuso S., Volkmann D., Eds. Berlin Heidelberg: Springer-Verlag, pp. 291–308.
7. Fromm J., Spanswick R. 1993. Characteristics of action potentials in willow (*Salix viminalis L.*). *J. Exp. Bot.* **44**, 1119–1125.
8. Felle H.H., Zimmermann M.R. 2007. Systemic signalling in barley through action potentials. *Planta*. **226**, 203–214.
9. Król E., Dziubińska H., Trebacz K. 2010. What do plants need action potentials for? In: *Action potential: Biophysical and cellular context, initiation, phases and propagation*. DuBois M.L., Ed. New York: Nova Sci. Publ., pp. 1–26.
10. Shiina T., Tazawa M. 1986. Action potential in *Luffa cylindrical* and its effects on elongation growth. *Plant Cell. Physiol*. **27**, 1081–1089.
11. Trebacz K., Dziubinska H., Król E. 2006. Electrical signals in longdistance communication in plants. In: *Communication in plants. Neuronal aspects of plant life.* Baluska F., Mancuso S., Volkmann D., Eds. Berlin: Springer, pp. 277–290.
12. Retivin V.G., Opritov V.A., Abramova N.N., Lobov S.A., Fedulina S.B. 1999. The ATP level in phloem exudates from the stem of a higher plant after the propagation of electrical responses to burn and cooling. *Vestn. Nizhegorodskogo universiteta im. N.I. Lobachevskogo. Biology series*. (Rus.). **1**, 124–131.
13. Surova L., Sherstneva O., Vodeneev V., Katicheva L., Semina M., Sukhov V. 2016. Variation potential-induced photosynthetic and respiratory changes increase ATP content in pea leaves. *J. Plant Physiol.* **202**, 57–64. doi 10.1016/j.jplph.2016.05.024
14. Fromm J., Lautner S. 2007. Electrical signals and their physiological significance in plants. *Plant Cell Environ.* **30**, 249–257.
15. Sinyukhin A.M. 1973. Functional activity of action potential in ferns and mosses during fertilization. *Biofizika* (Rus.). **18**, 477–482.
16. Sukhov V. 2016. Electrical signals as mechanism of photosynthesis regulation in plants. *Photosynth. Res.* **130**, 373–387. doi 10.1007/s11120-016-0270-x
17. Koziolek C., Grams T.E.E., Schreiber U., Matyssek R., Fromm J. 2004. Transient knockout of photosynthesis mediated by electrical signals. *New Phytol*. **161**, 715–722.
18. Lautner S., Grams T.E.E., Matyssek R., Fromm J. 2005. Characteristics of electrical signals in poplar and responses in photosynthesis. *Plant Physiol*. **138**, 2200–2209.
19. Pavlovič A., Slováková L., Pandolfi C., Mancuso S. 2011. On the mechanism underlying photosynthetic limitation upon trigger hair irritation in the carnivorous plant Venus flytrap (*Dionaea muscipula Ellis*). *J. Exp. Bot.* **62**, 1991–2000.
20. Dziubinska H., Trebacz K., Zawadzki T. 1989. The effect of excitation on the rate of respiration in the liverwort *Conocephalum conicum*. *Physiol. Plant.* **75**, 417–423.
21. Retivin V.G., Opritov V.G., Fedulina S.B. 1997. Action potential-induced preadaptation of tissues of the *Cucurbita pepo* stem to the damaging effect of low temperatures. *Fiziologiya rasteniy* (Rus.). **44**, 499–510.
22. Opritov V.A. 1998. *Funktsional'nye aspekty bioelektrogeneza u vysshikh rasteniy. 59-e Timiryazevskoye chteniye* (Functional aspects of bioelectrogenesis in higher plants. The 59th Timiryazev readings). Nizhny Novgorod: NNGU.
23. Sukhov V., Surova L., Sherstneva O., Bushueva A., Vodeneev V. 2015. Variation potential induces decreased PSI damage and increased PSII damage under high external temperatures in pea. *Funct. Plant Biol*. **42**, 727–736.
24. Surova L., Sherstneva O., Vodeneev V., Sukhov V. 2016. Variation potential propagation decreases heat-related damage of pea photosystem I by 2 different pathways. *Plant Sign. Behav.* **11**, e1145334.
25. Vodeneev V.A., Opritov V.A., Pyatygin S.S. 2006. Reversible change in intracellular pH during action potential generation in the higher plant *Cucurbita pepo. Russ. J. Plant Physiol.* **53**, 538–545.
26. Swarbreck S.M., Colaço R., Davies J.M. 2013. Plant calcium-permeable channels. *Plant Physiol*. **163**, 514–522.
27. Jammes F., Hu H.-C., Villiers F., Bouten R., Kwak J.M. 2011. Calcium-permeable channels in plant cells. *FEBS J*. **278**, 4262–4276.
28. Plieth C. 1999. Temperature sensing by plants: Calcium-permeable channels as primary sensors – a model. *J. Membr. Biol*. **172**, 121–127.
29. Carpaneto A., Ivashikina N., Levchenko V., Krol E., Jeworutzki E., Zhu J.-K., Hedrich R. 2007. Cold transiently activates calcium-permeable channels in *Arabidopsis* mesophyll cells. *Plant Physiol.* **143**, 487–494.
30. Trebacz K., Tarnecki R., Zawadzki T. 1989. The effect of ionic channel inhibitors and factors modifying metabolism on the excitability of the liverwort *Conocephalum conicum*. *Physiol. Plant.* **75**, 24–30.
31. Krol E., Dziubińska H., Trebacz K. 2004. Low-temperature-induced transmembrane potential changes in mesophyll cells of *Arabidopsis thaliana, Helianthus annuus* and *Vicia faba*. *Physiol. Plant.* **120**, 265–270.
32. Lewis B.D., Karlin-Neumann G., Davis R.W., Spalding E.P. 1997. Ca^{2+}-activated anion channels and membrane depolarizations induced by blue light and cold in *Arabidopsis* seedlings. *Plant Physiol.* **114**, 1327–1334.
33. Opritov V.A., Pyatygin S.S., Vodeneev V.A. 2002. Direct coupling of generation in the cells of the higher plant *Cucurbita pepo* L. with the work of electrogenic pump. *Russ. J. Plant Physiol*. **49**, 534–542.
34. Shimmen T., Mimura T., Kikuyama M., Tazawa M. 1994. Characean cells as a tool for studying electrophysiological characteristics of plant cell structure and function. *Cell Struct. Funct.* **19**, 263–278.
35. Beilby M.J. 2007. Action potential in charophytes. *Int. Rev. Cytol.* **257**, 43–82.
36. Kikuyama M., Tazawa M. 1976. Tonoplast action potential in *Nitella* in relation to vacuolar chloride concentration. *J. Membr. Biol*. **29**, 95–110.

37. Hedrich R. 2012. Ion channels in plants. *Physiol. Rev.* **92**, 1777–1811.

38. Isayenkov S., Isner J.C., Maathuis F.J.M. 2010. Vacuolar ion channels: Roles in plant nutrition and signaling. FEBS Lett. **584**, 1982–1988.

39. Reisen D., Marty F., Leborgne-Castel N. 2005. New insights into the tonoplast architecture of plant vacuoles and vacuolar dynamics during osmotic stress. *BMC Plant Biol.* **5**, 13.

40. Marty F. 1999. Plant vacuoles. *Plant Cell.* **11**, 587–599.

41. Stael S., Wurzinger B., Mair A., Mehlmer N., Vothknecht U.C., Teige M. 2012. Plant organellar calcium signalling: An emerging field. *J. Exp. Bot.* **63**, 1525–1542.

42. Barkla B.J., Pantoja O. 1996. Physiology of ion transport across the tonoplast of higher plants. *Annu. Rev. Plant Physiol. Plant Mol. Biol.* **47**, 159–184.

43. Biskup B., Gradmann D., Thiel G. 1999. Calcium release from $InsP_3$-sensitive internal stores initiates action potential in Chara. *FEBS Lett.* **453**, 72–76.

44. Wacke M., Thiel G., Hütt M.-T. 2003. Ca^{2+} dynamics during membrane excitation of green alga *Chara*: Model simulations and experimental data. *J. Membr. Biol.* **191**, 179–192.

45. Beilby M.J. 1982. $C1^-$ channels in Chara. *R. Soc. London B.* **299**, 435–445.

46. Mummert H., Gradmann D. 1991. Action potentials in *Acetabularia*: Measurement and simulation of voltage-gated fluxes. *J. Membr. Biol.* **124**, 265–273.

47. Gradmann D., Blatt M.R., Thiel G. 1993. Electrocoupling of ion transporters in plants. *J. Membr. Biol.* **136**, 327–332.

48. Gradmann D., Johannes E., Hansen U.-P. 1997. Kinetic anaylsis of Ca^{2+}/K^+ selectivity of an ion channel by single-binding-site models. *J. Membr. Biol.* **159**, 169–178.

49. Gradmann D. 2001. Impact of apoplast volume on ionic relations in plant cells. *J. Membr. Biol.* **184**, 61–69.

50. Sukhov V., Vodeneev V. 2009. Mathematical model of action potential in cells of vascular plants. *J. Membr. Biol.* **232**, 59–67.

51. Sukhov V., Nerush V., Orlova L., Vodeneev V. 2011. Simulation of action potential propagation in plants. *J. Theor. Biol.* **291**, 47–55.

52. Hodgkin A.L., Huxley A.F. 1952. A quantitative description of membrane current and its application to conduction and excitation in nerve. *J. Physiol.* **117**, 500–544.

53. Schroeder J.I., Fang H.H. 1991. Inward-rectifying K^+ channels in guard cells provide a mechanism for low-affinity K^+ uptake. *Proc. Natl. Acad. Sci. USA.* **88**, 11583–11587.

54. Piñeros M., Tester M. 1996. Calcium channels in higher plant cells: Selectivity, regulation and pharmacology. *J. Exp. Bot.* **48**, 551–577.

55. White P.J., Davenport R.J. 2002. The voltage-independent cation channel in the plasma membrane of wheat roots is permeable to divalent cations and may be involved in cytosolic Ca^{2+} homeostasis. *Plant Physiol.* **130**, 1386–1395.

56. Halm D.R., Frizzell R.A. 1992. Anion permeation in an apical membrane chloride channel of a secretory epithelial cell. *J. Gen. Physiol.* **99**, 339–366.

57. Nayyar H. 2003. Calcium as environmental sensor in plants. *Curr. Sci.* **84**, 893–902.

58. Wacke M., Thiel G. 2001. Electrically triggered all-or-none Ca^{2+}-liberation during action potential in the giant alga Chara. *J. Gen. Physiol.* **118**, 11–21.

59. DeWald D.B., Torabinejad J., Jones C.A, Shope J.C., Cangelosi A.R, Thompson J.E., Prestwich G.D., Hama H. 2001. Rapid accumulation of phosphatidylinositol 4,5-bisphosphate and inositol 1,4,5-trisphosphate correlates with calcium mobilization in salt-stressed *Arabidopsis. Plant Physiol.* **126**, 759–769.

60. Hansen U.-P., Gradmann D., Sanders D., Slayman C.L. 1981. Interpretation of current–voltage relationships for "active" ion transport systems: I. Steady-state reaction-kinetic analysis of class-I mechanisms. *J. Membr. Biol.* **63**, 165–190.

61. Gradmann D., Boyd C.M. 2005. Apparent charge of binding site in ion-translocating enzymes: Kinetic impact. *Eur. Biophys. J.* **34**, 353–357.

62. Pfanz H., Heber U. 1986. Buffer capacities of leaves, leaf cells, and leaf cell organelles in relation to fluxes of potentially acidic gases. *Plant Physiol.* **81**, 597–602.

63. Tuteja N. 2009. Integrated calcium signaling in plants. In: *Signaling in Plants.* Baluska F., Mancuso S., Eds. Berlin–Heidelberg: Springer-Verlag, pp. 29–40.

64. Liu J., Whalley H.J., Knight M.R. 2015. Combining modelling and experimental approaches to explain how calcium signatures are decoded by calmodulin-binding transcription activators (CAMTAs) to produce specific gene expression responses. *New Phytol.* **208**, 1–14.

65. Barbier-Brygoo H., Vinauger M., Colcombet J., Ephritikhine G., Frachisse J.-M., Maurel C. 2000. Anion channels in higher plants: Functional characterization, molecular structure and physiological role. *Biochim. Biophys. Acta.* **1465**, 199–218.

66. Randall S.K. 1992. Characterization of vacuolar calcium-binding proteins. *Plant Physiol.* **100**, 859–867.

67. Greenwald I. 1938. The dissociation of some calcium salts. *J. Biol. Chem.* **124**, 437–452.

68. Colcombet J., Thomine S., Guern J., Frachisse J.-M., Barbier-Brygoo H. 2001. Nucleotides provide a voltage-sensitive gate for the rapid anion channel of *Arabidopsis* hypocotyl cells. *J. Biol. Chem.* **276**, 36139–36145.

69. Zhang W.-H., Walker N.A., Patrick J.W., Tyerman S.D. 2004. Pulsing Cl^- channels in coat cells of developing bean seeds linked to hypo-osmotic turgor regulation. *J. Exp. Bot.* **55**, 993–1001.

70. Berestovsky G.N., Kataev A.A. 2005. Voltage-gated calcium and Ca^{2+}-activated chloride channels and Ca^{2+} transients: Voltage-clamp studies of perfused and intact cells of Chara. *Eur. Biophys. J.* **34**, 973–986.

71. Brüggemann L., Dietrich P., Becker D., Dreyer I., Palme K., Hedrich R. 1999. Channel-mediated high-affinity K^+ uptake into guard cells from *Arabidopsis. Proc. Natl. Acad. Sci. USA.* **96**, 3298–3302.

72. Hills A., Chen Z.-H., Amtmann A., Blatt M.R., Lew V.L. 2012. OnGuard, a Computational platform for quantitative kinetic modeling of guard cell physiology. *Plant Physiol.* **159**, 1026–1042.

73. Kinoshita T., Nishimura M., Shimazakib K. 1995. Cytosolic concentration of Ca^{2+} regulates the plasma membrane H^+-ATPase in guard cells of Fava bean. *Plant Cell*. **7**, 1333–1342.
74. Tikhonova L.I., Pottosin I.I., Dietz K.-J., Schbnknecht G. 1997. Fast-activating cation channel in barley mesophyll vacuoles. Inhibition by calcium. *Plant J.* **11**, 1059–1070.
75. Gobert A., Isayenkov S., Voelker C., Czempinski K., Maathuis F.J. M. 2007. The two-pore channel TPK1 gene encodes the vacuolar K^+ conductance and plays a role in K^+ homeostasis. *Proc. Natl. Acad. Sci. USA*. **104**, 10726–10731.
76. Alexandre J., Lassalles J.P., Kado R.T. 1990. Opening of Ca^{2+} channels in isolated red beet root vacuole membrane by inositol 1,4,5-trisphosphate. *Nature*. **343**, 567–570.
77. Plant P.J., Gelli A., Blumwald E. 1994. Vacuolar chloride regulation of an anion-selective tonoplast channel. *J. Membr. Biol*. **140**, 1–12.
78. Hafke J.B., Hafke Y., Smith J.A.C., Lüttge U., Thiel G. 2003. Vacuolar malate uptake is mediated by an anion-selective inward rectifier. *Plant J.* **35**, 116–128.
79. Gambale F., Kolb H.A., Cant A.M., Hedrieh R. 1994. The voltage-dependent H^+-ATPase of the sugar beet vacuole is reversible. *Eur. Biophys. J.* **22**, 399–403.
80. Davies J. M., Hunt I., Sanders D. 1994. Vacuolar H^+-pumping ATPase variable transport coupling ratio controlled by pH. *Plant Biol.* **91**, 8547–8551.
81. Askerlund P., Evans D.E. 1992. Reconstitution and characterization of a calmodulin-stimulated Ca^{2+}-pumping ATPase purified from *Brassica oleracea* L. *Plant Physiol*. **100**, 1670–1681.
82. Martinoia E., Maeshima M., Neuhaus H.E. 2007. Vacuolar transporters and their essential role in plant metabolism. *J. Exp. Bot*. **58**, 83–102.
83. Etxeberria E., Pozueta-Romero J., Gonzalez P. 2012. In and out of the plant storage vacuole. *Plant Sci*. **190**, 52–61.
84. Davies J.M. 1996. Vacuolar energization: Pumps, shunts and stress. *J. Exp. Bot*. **48**, 633–641.
85. Sherstneva O.N., Vodeneev V.A., Katicheva L.A., Surova L.M., Sukhov V.S. 2015. Involvement of the changes in intra- and extracellular pH in the development of variable potential-induced photosynthetic response in pumpkin sprouts. *Biochemistry* (*Mosc*.). **80**, 776–784.
86. Pyatygin S.S., Opritov V.A., Khudyakov V.A. 1992. Subthreshold changes in excitable membranes of *Cucurbita pepo* L. stem cells during cooling-induced action-potential generation. *Planta*. **186**, 161–165.
87. Opritov V.A., Lobov S.A., Pyatygin S.S., Mysyagin S.A. 2005. Analysis of possible involvement of local bioelectric responses in chilling perception by higher plants exemplified by *Cucurbita pepo. Russ. J. Plant Physiol*. **52** (6), 801–808.
88. Krol E., Dziubinska H., Stolarz M., Trebacz K. 2006. Effects of ion channel inhibitors on cold and electrically induced action potentials in *Dionaea muscipula*. *Biol. Plant*. **50**, 411–416.
89. Pyatygin S.S., Opritov V.A., Polovinkin A.V., Vodeneev V.A. 1999. On the nature of action potential of the higher plants. *Dokl. Akademii nauk* (Rus.). **366**, 404–407.
90. Vodeneev V.A., Sherstneva O.N., Surova L.M., Semina M.M., Katicheva L.A., Sukhov V.S. 2016. Age-dependent changes of photosynthetic responses induced by electrical signals in wheat seedlings. *Russ. J. Plant Physiol*. **63** (6), 861–868.

Translated by E.V. Makeeva